

*Applying Regular Perturbation Analysis to HCV Viral Load Equations

Jeffrey Saltzman[†] Robert Nachbar[†] Paul Panorchan[‡] Julie Stone[‡] Anis Khan[§]

March 16, 2010

Abstract

There are many mathematical, time-dependent models of hepatitis type C virus (HCV) infection found in the literature. Although the evolution of the level of infection is complex, there are many successful models explaining a variety of *in-vivo* and *in-vitro* observations. These models are playing a pivotal role in the pharmaceutical industry by helping researchers and clinicians analyze the performance of HCV therapeutics. New treatments of HCV quickly drive the amount of virus in the body below measurable levels. This leaves few data points for researchers to fit models. Using regular perturbation methodologies we derive and compare a series of approximations for a standard model to understand tradeoffs between model complexity (number of parameters) and model accuracy. This interplay between perturbation analysis and numerical methods leads to numerical and analytical methods yielding superior insight into the sparse data generated from new treatment regimes.

1 Introduction

The World Health Organization (WHO) estimates approximately 170 million people, world-wide, are infected by HCV. Further, the WHO asserts between 3 and 4 million persons are newly infected each year. HCV is attributed to be the major cause of acute hepatitis and chronic liver disease, including cirrhosis and liver cancer [1].

Treatment of HCV is expensive, of long duration and of limited effectiveness [2]. In the past several years pharmaceutical companies and biotechs motivated to improve on outcomes from currently practiced treatment regimes, known as standard of care, have been engaged in developing second generation therapeutics promising shorter treatment intervals with fewer side-effects and greater efficacy [3].

Mathematical modeling has played an important role in the understanding of disease progression and treatment. In addition, mathematical modeling is becoming a fundamental tool for the development of new therapeutics in the pharmaceutical industry. These

models contribute to many aspects of drug development ranging from knowledge management to dose selection to clinical trial design. Taking all these aspects together, it is easy to see modeling as becoming an important decision aid in the pharmaceutical industry.

Models predicting viral load, the number concentration of viruses in the blood plasma or liver, are of central focus of modeling in the HCV disease area. Viral load models are of importance because current assays are not able to detect viral ribonucleic acid (RNA) below a significant non-zero threshold. RNA signatures are the primary way viruses are accounted for. This limit is called the level of quantitation (LOQ). Current published levels of detection are described in [4]. It is known that viral load levels must drop several orders of magnitude below LOQ in order to attain a sustained viral load response (SVR) or cure. Modeling currently provides the only plausible window into this regime of treatment.

Modeling methodologies used are diverse and are tailored to available data and application [5, 6, 7]. Mathematical models are taxonomized by the number different mutations of the HCV virus handled, the duration the simulation is designed to accurately model and whether the consideration of viral replication dynamics within the hepatocyte (liver cell) is considered. Our focus is on a single-viral-species, multi-phase model for simplicity of exposition although much of this analysis may be extended to more complex models.

In the next section we introduce the equations describing a single-viral-species kinetics model. We apply regular perturbation analysis, functional iteration and the two-scale method of Cole and Kevorkian [8], [9] to find a series of approximations to the solutions of the differential equations. Using these results we compare the series of approximations for this standard model to understand tradeoffs between model complexity (number of parameters) and model accuracy. We then analyze this approximation hierarchy and how it elucidates the behavior of viral dynamics. Overall, this interplay between perturbation and numerical analysis leads to *both* new numerical and analytical methodologies. Together, these new methodologies yield superior insight into the

*Merck manuscript 2009-MS-4226

[†]Applied Computer Science and Mathematics, Merck Research Laboratory, Rahway, NJ.

[‡]Clinical Pharmacokinetics and Drug Metabolism, Merck Research Laboratory, West Point, PA.

[§]Quantitative Clinical Pharmacology, Merck Research Laboratory, Rahway, NJ.

sparse data generated from new treatment regimes. We demonstrate how these models' applications may be applied to synthetic and real clinical data.

2 Single Species Equations

We use a compartmental model to explain the dynamics of the hepatitis C virus. Our model follows the work of Neumann and Perelson [5].

2.1 Three Compartment Model The model schematic is shown in Figure 1. It has three compartments representing the viral number density (V), the infected cell number density (I) and the uninfected cell number density (U). V is generally called the viral load.

The change in the viral load in the system is influenced by several factors. First, viral clearance is modeled by a constant rate, c , and is proportional to the amount of virus present. New viruses are introduced from infected cells with a rate constant p and in proportion to the number of infected cells. Viral production may be reduced through treatment modeled by the term $(1 - \varepsilon)$. ε is a function of an antiviral drug concentration described by one or more pharmacokinetics equations.

Prior to treatment ε is zero and after treatment begins we assume it is a fixed value in the interval $[0, 1)$. Infected cells have a clearance rate constant δ and clear in proportion to the number of infected cells. We assume a rapid cell regeneration rate, ρ , constraining the total number of hepatocytes to a fixed constant H_0 . Evidence is found for this assumption in Michalopoulos and DeFrances [10]. The article shows observations of both rapid liver regeneration after resection and a stable tissue volume under quiescent conditions. Finally, the product of the viral load and the number of available uninfected cells determines the rate of increase of infected cells in proportion to β . This flux is modulated by the term $(1 - \eta)$ due to treatment. η is zero prior to treatment and is fixed in an interval $[0, 1)$ after treatment begins. Like antivirals, η is a function of anti-infective drug concentration. The differential equations associated with the viral kinetics diagram are

$$(2.1) \quad \frac{dV}{dt} = -cV + (1 - \varepsilon)pI,$$

$$(2.2) \quad \frac{dI}{dt} = -\delta I + (1 - \eta)\beta V U,$$

and

$$(2.3) \quad H_0 = I + U.$$

2.2 Steady-state Simplifications We first rescale dependent and independent variables in (2.1), (2.2), and (2.3) in order to reduce the number of parameters in the

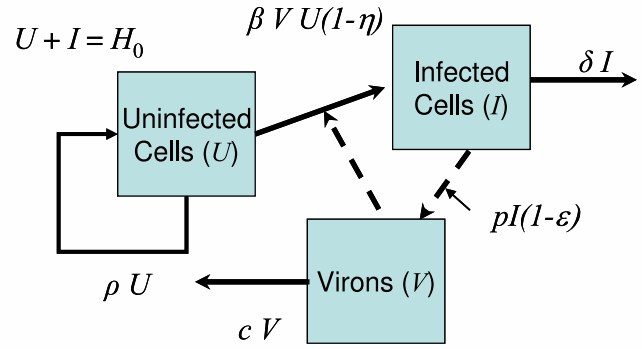


Figure 1: Single species compartmental model for HCV viral dynamics.

system of equations. The first step in this process is to define new dependent variables

$$i = \frac{I}{H_0} \quad \text{and} \quad v = \frac{V}{V_0},$$

where V_0 is the viral load prior to treatment. We use (2.3) to eliminate U from (2.1) and (2.2)

$$(2.4) \quad \frac{dv}{dt} = -cv + (1 - \varepsilon) \frac{pH_0}{V_0} i,$$

$$(2.5) \quad \frac{di}{dt} = -\delta i + (1 - \eta) \beta V_0 v (1 - i).$$

Equations (2.4) and (2.5) have steady-state solutions found by setting the time derivatives to zero. Although disease progression is observed to have steadily increasing viral loads, the rate of progression is sufficiently slow as to warrant using the so called “quasi-steady-state” approximation [5] to find initial conditions. Assume an initial viral load ($v(0) = v_0 = 1$), an infected cell fraction ($i(0) = i_0$) and no drug presence ($\varepsilon = \eta = 0$) prior to treatment for steady-state conditions. Using these assumptions

$$(2.6) \quad \frac{pH_0}{V_0} = \frac{c}{i_0},$$

$$(2.7) \quad \beta V_0 = \frac{\delta i_0}{(1 - i_0)}.$$

Using (2.6) and (2.7) in (2.4) and (2.5) we find equations with dimensionless dependent variables

$$(2.8) \quad \frac{dv}{dt} = -cv + (1 - \varepsilon) c \frac{i}{i_0},$$

$$(2.9) \quad \frac{di}{dt} = -\delta i + (1 - \eta) \delta i_0 v \frac{(1 - i)}{(1 - i_0)}.$$

2.3 Rescaling the Independent Variable Time scales of interest in viral kinetics are the viral clearance time (c^{-1}) and the infected cell clearance time (δ^{-1}). Viral clearance rates are measured in hours while infected cell clearance rates are measured in days. The equations are scaled to the fastest time, c , by introducing new variables

$$T = ct \quad \text{and} \quad \omega = \frac{\delta}{c}.$$

Using the chain rule the differential equations are written using the new time variable T as

$$(2.10) \quad \frac{dv}{dT} = -v + (1 - \varepsilon) \frac{i}{i_0},$$

$$(2.11) \quad \frac{di}{dT} = -\omega i + \omega(1 - \eta) v i_0 \frac{(1 - i)}{(1 - i_0)},$$

where ω is considered a small parameter as $c \gg \delta$.

2.4 Numerical Solution Figure 2 shows a representative numerical solution of equations (2.10) and (2.11) with parameters $\omega = 0.1$, an efficacy $\varepsilon = 0.96$ and initial infection fraction $i_0 = 0.85$. The first red region from the left is the quasi-steady-state solution. The adjoining blue region shows the biphasic decline of the viral load. The second phase is often called the “ δ ” phase emphasizing clearance of hepatocytes as the dominant process. The thin red region is a result of an artificially rapid change of efficacy and is usually broader for realistic drug treatments. The next right blue region shows a slower rebound interval (limited by the slower of infection or viral production rates) leading to the original quasi-steady-state (the equations have memory). Clinical assays currently have a limited sensitivity with respect to viral loads indicated by the horizontal line. If the efficacy is very near one or viral loads are not large to begin with, the second phase of the viral decline may not be observed.

3 Analysis

Using regular perturbation analysis and functional iteration, we examine the behavior of equations (2.10) and (2.11) at three different time scales. These time scales are small ($\sim c^{-1}$), large ($\sim \delta^{-1}$) and steady-state (infinite) time scales. Neither regular perturbation analysis nor functional iteration yields a *uniform approximation* for all time. For this need we turn to two-scale methods.

3.1 Steady-state Analysis and Cure Boundaries

By examining the algebraic relations found by setting the derivatives to zero in equations (2.10) and (2.11) we are able to understand when viral load and infected cell

fractions have zero or negative limit values. A necessary condition for SVR is

$$(3.12) \quad s = \frac{(1 - \varepsilon)(1 - \eta)}{1 - i_0} \leq 1.$$

Although there are no time scales suggested by (3.12), as the left hand side of the inequality becomes smaller, we will see later in this paper the *rate of approach* to SVR is faster. A key observation is as the initial infected cell fraction, i_0 , approaches one it becomes more difficult to attain SVR. Difficulty means finding therapeutics with efficacies approaching one.

The inequality reveals a synergistic relation between anti-infectives and antivirals. A small value in the numerator of (3.12) may be achieved by choosing either η or ε near one and the other zero (monotherapy) or use lesser values for both parameters with the same product (combination therapy). For example, lets assume an antiviral needs to reach an efficacy of $\varepsilon = .96$ in order to attain an SVR alone ($\eta = 0$). Used in conjunction with a mildly effective anti-infective, $\eta = 0.75$, ε need only have a value of 0.84. If ε remains at a value of 0.96 and an anti-infective is added to the mix, the computed efficacy of the combination is 0.99. Here effective efficacy is the value necessary for either an antiviral or anti-infective alone (monotherapy) to have the same denominator in (3.12).

3.2 Regular Perturbation Analysis We assume expansions of the form

$$(3.13) \quad v(T, \omega) = v^{(0)}(T) + \omega v^{(1)}(T) + \omega^2 v^{(2)}(T) + \dots + \omega^N v^{(N)}(T) + R_{v,N}(T, \omega),$$

$$(3.14) \quad i(T, \omega) = i^{(0)}(T) + \omega i^{(1)}(T) + \omega^2 i^{(2)}(T) + \dots + \omega^N i^{(N)}(T) + R_{i,N}(T, \omega),$$

where

$$R_{v,N}(T, \omega) \sim R_{i,N}(T, \omega) \sim O(\omega^{N+1}).$$

Inserting (3.13) and (3.14) into (2.10) and (2.11) and collecting coefficients of like powers of ω produces a series of systems of linear differential equations that may be solved successively:

$$(3.15) \quad \frac{dv^{(0)}}{dT} = -v^{(0)} + (1 - \varepsilon) i^{(0)}/i_0,$$

$$(3.16) \quad \begin{aligned} v^{(0)}(0) &= 1. \\ \frac{di^{(0)}}{dT} &= 0, \end{aligned}$$

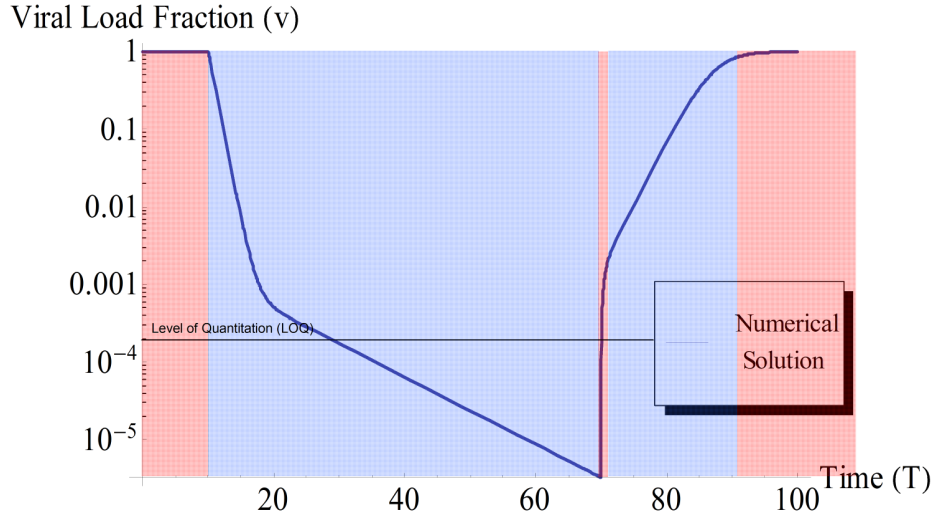


Figure 2: Various treatment phases and the corresponding time evolution of viral load.

$$i^{(0)}(0) = i_0,$$

$$(3.17) \quad \frac{dv^{(1)}}{dT} = -v^{(1)} + (1 - \varepsilon)i^{(1)}/i_0,$$

$$v^{(1)}(0) = 0.$$

$$(3.18) \quad \frac{di^{(1)}}{dT} = -i^{(0)} + (1 - \eta)i_0v^{(0)} \frac{(1 - i^{(0)})}{(1 - i_0)},$$

$$i^{(1)}(0) = 0.$$

⋮

3.3 Functional Iteration The regular perturbation method suggests the application of functional iteration to (2.10) and (2.11). Here the nonlinear terms are lagged enabling analytic solutions to all orders:

$$(3.19) \quad \frac{dv_f^{(j)}}{dT} = -v_f^{(j)} + (1 - \varepsilon)i_f^{(j-1)}/i_0,$$

$$(3.20) \quad \frac{di_f^{(j)}}{dT} = -\omega i_f^{(j)} + \omega i_0(1 - \eta)v_f^{(j-1)} \frac{(1 - i_f^{(j-1)})}{(1 - i_0)},$$

where

$$v_f(0)^{(j)} = 1, \quad i_f(0)^{(j)} = i_0 \quad \text{for } j = 0, 1, 2, \dots$$

and an initial iterate

$$v_f^{(0)}(T) = 1 \quad \text{and} \quad i_f^{(0)}(T) = i_0.$$

The iteration is rapidly convergent for $\omega \ll 1$. Proof of convergence and bounds on the rate of convergence may be derived from an application of the Picard-Lindelöf theorem [11]. Our work on understanding the viral dynamics equations originally started with functional iteration. We quickly found regular perturbation analysis more useful because of its ability to formally separate expansion terms in powers of ω .

3.4 Fast Time Scales Using the zero order expansion from regular perturbation equations, (3.15) and (3.16), we are able to derive the well-known viral load equation for short times

$$(3.21) \quad v^{(0)}(T) = e^{-T} + (1 - \varepsilon)(1 - e^{-T}),$$

$$(3.22) \quad i^{(0)}(T) = i_0.$$

Note that any effect of the anti-infective ($\eta \neq 0$) is not seen for short time scales. The functional iteration's initial function values are designed to mimic this behavior. The solutions from the first functional iteration are

$$(3.23) \quad v_f^{(1)}(T) = e^{-T} + (1 - \varepsilon)(1 - e^{-T}),$$

$$(3.24) \quad i_f^{(1)}(T) = i_0 (e^{-\omega T} + (1 - \eta)(1 - e^{-\omega T})).$$

The functional iteration includes a slow time scale decay to the value $i_0(1 - \eta)$. The viral load solutions are identical. In fitting data for 1-2 days both solutions justify treating i_0 as a constant.

3.5 Longer (Slow) Time Scales We examine the next term in the regular expansion by solving (3.17) and (3.18). These are

$$(3.25) \quad v^{(1)}(T) = -T \left((1 - \varepsilon)\varepsilon^* + (1 - \varepsilon^*)\varepsilon e^{-T} \right) + \left((1 - e^{-T})((1 - \varepsilon)\varepsilon^* + (1 - \varepsilon^*)\varepsilon) \right),$$

$$(3.26) \quad i^{(1)}(T) = -i_0 \left(\varepsilon^* T - (1 - \eta)\varepsilon(1 - e^{-T}) \right),$$

where the effective efficacy, ε^* is defined through the relation

$$(1 - \varepsilon^*) = (1 - \varepsilon)(1 - \eta).$$

The expansion is not *uniform* for all T . The viral load expansions are independent of i_0 .

The second iterate of the functional iteration yields more complex solutions

$$(3.27) \quad v_f^{(2)}(T) = e^{-T} + (1 - \varepsilon^*)(1 - e^{-T}) + \frac{(1 - \varepsilon)\eta}{(1 - \omega)} (e^{-\omega T} - e^{-T}),$$

$$(3.28) \quad i_f^{(2)}(T) = i_0 \left[e^{-\omega T} + \frac{(1 - \varepsilon^*)(1 - i_0(1 - \eta))}{(1 - i_0)} (1 - e^{-\omega T}) + \frac{\omega\varepsilon(1 - \eta)(1 - i_0(1 - \eta))}{(1 - \omega)(1 - i_0)} (e^{-\omega T} - e^{-T}) - \frac{\omega\varepsilon\eta(1 - \eta)}{(1 - i_0)} (e^{-\omega T} - e^{-(\omega+1)T}) - \frac{\omega\eta(1 - \varepsilon^*)}{(1 - i_0)} T e^{-\omega T} \right].$$

Like the regular expansion, the viral load functional iterate is independent of i_0 . The expansions so far derived indicate a hierarchy of influence of the various parameters. For short times only c and ε shape the evolution of the viral load. Higher order expansions show the influence of η and δ . Eventually i_0 appears in higher order terms.

The application of this observation is to find additional parameters δ and η without having to fit i_0 . This is useful in cases where antivirals and/or anti-infectives have high efficacy driving the viral load *near* the level of quantitation. Knowing where the fast time scales end is enough to fit these additional parameters. To carry out this program will require finding a time interval where both the influence of δ is felt and where the approximation expansion is valid.

3.6 Uniform Asymptotic Analysis As finding reliable, sharp bounds on the residuals of the expansions may be difficult, we instead look at uniform expansions

and tease out the effect of i_0 . Two-scale analysis assumes an explicit expansion of the solutions of (2.10) and (2.11) in both time scales leading to a series of recursively solved partial differential equations. We follow [9] by introducing the following solutions and expansions. Assume

$$(3.29) \quad v = v(T, \tau, \omega) \quad \text{and} \quad i = i(T, \tau, \omega)$$

where

$$(3.30) \quad \tau = \omega T.$$

This ansatz has the effect of separating the fast and slow time scales in the differential equations. Using the chain rule the resulting equations have the form

$$(3.31) \quad v_T + \omega v_\tau = -v + (1 - \varepsilon)i/i_0,$$

$$(3.32) \quad i_T + \omega i_\tau = -\omega i + \omega v i_0 \frac{(1 - i)}{1 - i_0}.$$

Assuming a regular¹ expansion of the form

$$(3.33) \quad v(T, \tau, \omega) = \overset{0}{v}(T, \tau) + \omega \overset{1}{v} + \dots + \omega^N \overset{N}{v} + R_{i, N+1}(T, \tau),$$

$$(3.34) \quad i(T, \tau, \omega) = \overset{0}{i}(T, \tau) + \omega \overset{1}{i} + \dots + \omega^N \overset{N}{i} + R_{i, N+1}(T, \tau),$$

and matching orders of ω we arrive at a series of partial differential equations grouped by matching powers of ω :

ω^0 :

$$(3.35) \quad \overset{0}{v}_T = -\overset{0}{v} + (1 - \varepsilon)\overset{0}{i}/i_0,$$

$$(3.36) \quad \overset{0}{i}_T = 0.$$

ω^1 :

$$(3.37) \quad \overset{1}{v}_T = -\overset{1}{v} - \overset{0}{v}_\tau + (1 - \varepsilon)\overset{1}{i}/i_0,$$

$$(3.38) \quad \overset{1}{i}_T = -\overset{0}{i} - \overset{0}{i}_\tau + (1 - \eta)i_0 \overset{0}{v} \frac{1 - \overset{0}{i}}{1 - i_0}.$$

ω^2 :

$$(3.39) \quad \overset{2}{v}_T = -\overset{2}{v} - \overset{1}{v}_\tau + (1 - \varepsilon)\overset{2}{i}/i_0.$$

$$(3.40) \quad \overset{2}{i}_T = -\overset{1}{i} - \overset{1}{i}_\tau + \frac{(1 - \eta)i_0}{(1 - i_0)} \left(\overset{1}{v}(1 - \overset{0}{i}) - \overset{0}{v} \overset{1}{i} \right).$$

¹The use in this section of the unusual looking notation containing indices centered above a variable such as $\overset{1}{v}(T, \tau)$ also follows [9]. The notation has advantages in both disambiguating itself from other expansion notation and leaving room for powers of variables.

⋮

The equations are solved in a stepwise process. First we examine the general solutions of (3.35) and (3.36).

$$(3.41) \quad \overset{0}{v} = A_0(\tau)e^{-T} + B_0(\tau)(1 - \varepsilon)(1 - e^{-T})/i_0,$$

$$(3.42) \quad \overset{0}{i} = B_0(\tau),$$

where

$$A_0(0) = 1 \quad \text{and} \quad B_0(0) = i_0.$$

In order to determine A_0 and B_0 for all τ it is necessary to examine the so-called *secular* terms in the first order expansion solutions of (3.37) and (3.38). These terms are easy to identify as contributing to unbounded growth of the solutions of the first order expansion equations. The general solution of the first order expansion equation for the infected cell fraction (3.38) has the form

$$(3.43) \quad \overset{1}{i} = B_1(\tau) + T(-B'_0(\tau) - B_0(\tau) + sB_0(\tau)(1 - B_0(\tau)) + e^{-T} \frac{i_0(1 - \eta)}{(1 - i_0)}(1 - B_0(\tau))(A_0(\tau) - (1 - \varepsilon)B_0(\tau)/i_0).$$

The unbounded secular term (the coefficients of T) may be zeroed by solving the differential equation

$$(3.44) \quad B'_0(\tau) = -B_0(\tau) + s(1 - B_0(\tau))B_0(\tau),$$

leading to the complete characterization of $B_0(\tau)$. Substituting B_0 into (3.37) yields a linear equation with a known forcing function. The solution has the form

$$(3.45) \quad \overset{1}{v} = A_1(\tau)e^{-T} - Te^{-T} \left[(A'_0(\tau) - (1 - \varepsilon)B'_0(\tau)/i_0) + s(1 - B(\tau))(A_0(\tau) - (1 - \varepsilon)B_0(\tau)/i_0) \right] + (1 - e^{-T}) \left[(B_1(\tau) - B_0(\tau)) \right].$$

$\overset{1}{v}$ has no secular terms so A_0 is chosen to simplify (3.45) by setting

$$(3.46) \quad A'_0(\tau) = (1 - \varepsilon)B'_0(\tau)/i_0.$$

Solving (3.44) and (3.46) completely specifies the solution of (3.35) and (3.36) such that

$$(3.47) \quad \overset{0}{v}(T) = \varepsilon e^{-T} + (1 - \varepsilon)B_0(\omega T)/i_0,$$

$$(3.48) \quad \overset{0}{i}(T) = B_0(\omega T),$$

where $B_0(\tau)$ has the form

$$(3.49) \quad B_0(\tau) = \begin{cases} \frac{i_0}{1 + i_0\tau} & \text{if } s = 1 \\ \frac{i_0(1 - s)}{e^{\tau(1-s)}(1 - (1 - i_0)s) - i_0s} & \text{otherwise.} \end{cases}$$

Notice the rate of decline in $B_0(\tau)$ and the corresponding rate of decline of $\overset{0}{i}(T)$ increase as $s \rightarrow 0$. Using the expression for s in (3.12), $B_0(\tau)$ may be expressed as

$$B_0(\tau) = \frac{i_0}{1 + \varepsilon\tau}$$

for small τ .

3.7 Comparison of Approximations Figure 3 shows a comparison of the approximations of the viral load equation — functional iteration, regular expansion and uniform expansion — to a numerical solution. Parameter values used are $\omega = .1$, $\eta = 0$, $\varepsilon = 0.95$ and $i_0 = 0.9$. Consequently $s = 0.5$. The figure roughly shows that the approximations are quite close to the numerical solution. To get a more quantitative picture we examine the relative error,

$$e_\alpha(t) = \frac{|v_\alpha(t) - v(t)|}{v(t)}$$

where “ α ” is a placeholder for any of the expansions discussed. Using the same parameter values as Figure 3 the relative errors of the fast and combined fast and slow terms of the regular perturbation approximations with respect to the numerical solution are shown in Figure 4. The uniform approximation error is included in this figure. We note that all the approximations with these parameters systematically overestimate the viral load. The time scale in this figure starts at 1.0 day in order to avoid the singularity at time 0.

4 Application

In this section we outline how these expansions may be used to find parameter estimates in short time data. In particular, intensively sampled viral load data may only be available for a few days or if the efficacy is sufficiently large for the viral load to quickly drop below LOQ.

The general approach is in steps. The first step is to fit the fast phase finding the parameters c and ε . The number of points used is minimized to ensure that only the fast phase contribution to the solution is fitted. This procedure is relatively simple in practice because the linearity of the log of the initial viral load decline may be examined numerically. Once these parameters are found we use the first order expansion parameters as

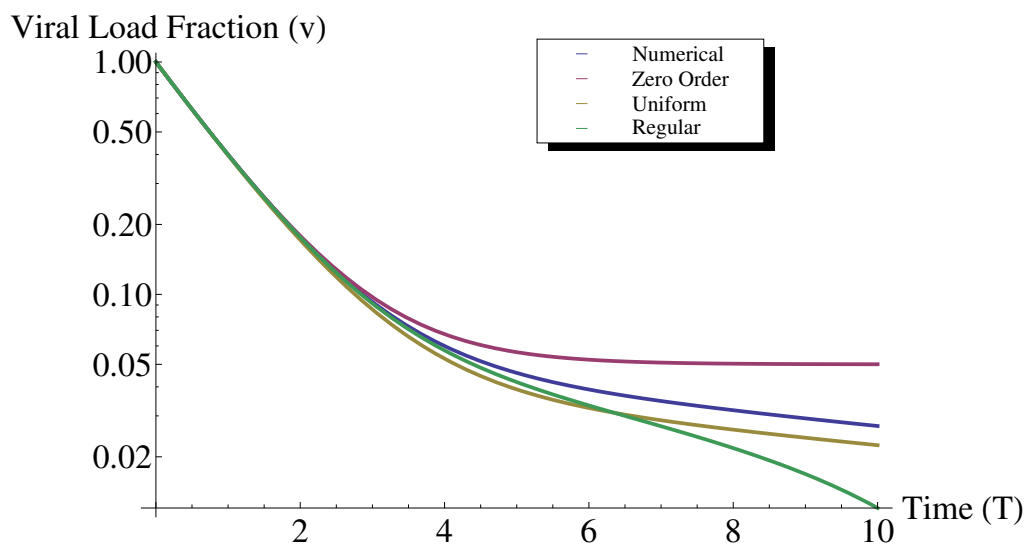


Figure 3: Various approximations of viral load.

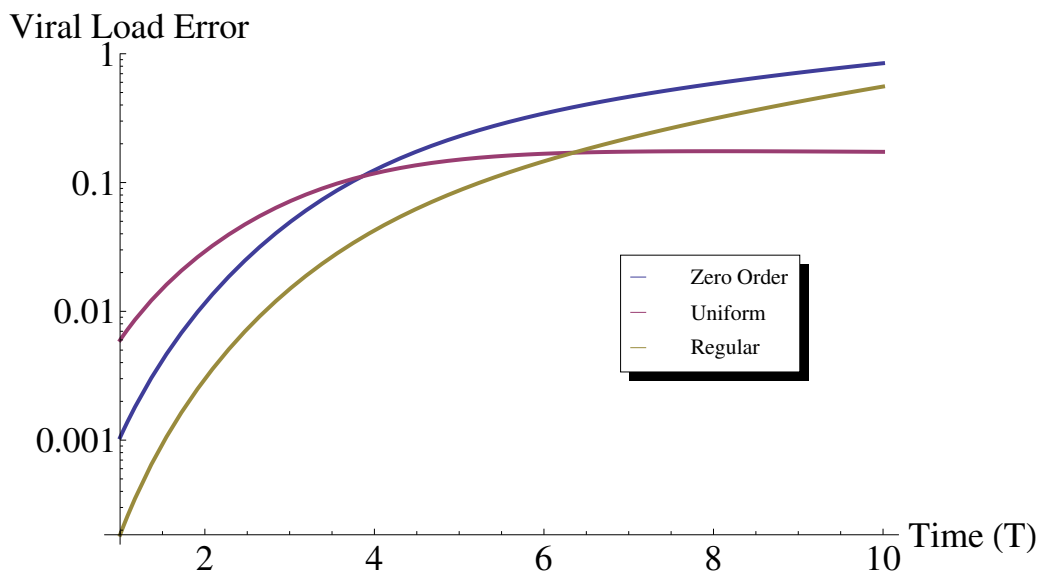


Figure 4: Relative error plots of the perturbation approximations.

	Est.	Std. Err.	t Stat.	P-Value
δ	0.365	0.0297	12.30	2.51×10^{-4}
ε	0.964	0.00154	622.77	3.99×10^{-11}
c	5.873	0.0501	117.14	3.18×10^{-8}

Table 1: Statistics for fit of the regular perturbation solution.

an initial guess to find δ . c is used to *unscale* the times in our analysis back to real time through the relation $T = ct$. If $c = 10$ and the interval $[0 < T < 4]$ is sufficiently small for using a first order approximation of the viral load then the map to an interval in real time is $[0 < t < 0.4]$.

4.1 Synthetic Data We examine a numerical solution of the equations (2.8) and (2.9) with parameter values $c = 6.0$, $\delta = 0.6$, $\varepsilon = 0.96$ and $i_0 = 0.85$. Viral loads are sampled from the numerical solution at times $0, 1/24, 1/12, 1/6, 1/3, 2/3, 4/3$. A set of time points such as these are called *intensively* sampled times as so many are taken in a single day. This type of sampling often occurs in early phase clinical trials. The logarithms of the viral load values are further perturbed by a normal distribution with standard deviation 0.025 to simulate noise found in the clinic. The resulting viral loads are fit using the *NonlinearModelFit* function found in *Mathematica*TM. Figure 5 visually exhibits a good fit over the entire range of times. The statistics in

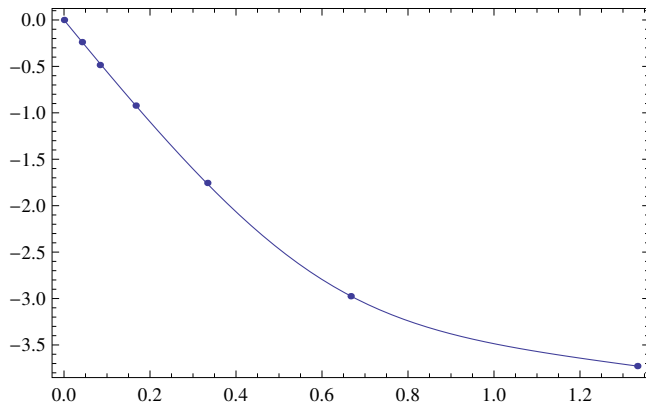


Figure 5: Plot of the perturbed data and model fit.

table 4.1 quantitatively indicate the fit is good. Notice δ is underestimated. The underestimate is due to using the regular perturbation solution as a model for times greater than $2/3$. The *approximation* error feeds back to the fitted parameters. Shortening the time interval will lead to instability of the fit with poor statistics. For

smaller δ and fixed c the approximation error improves, yielding both better statistics and more accurate estimates.

To examine variance in the estimators, 10,000 simulations are run to build distributions of all parameters. As might be expected the distributions show varying degrees of symmetry. Both the histograms for c and ε are symmetric while there is less symmetry in the histogram for δ .

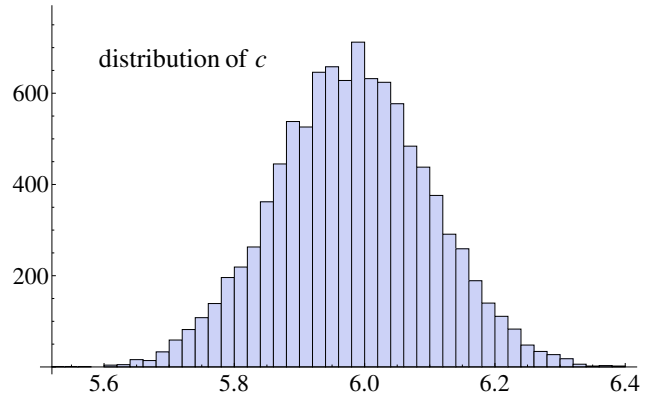


Figure 6: Histogram of 10,000 estimates of c .

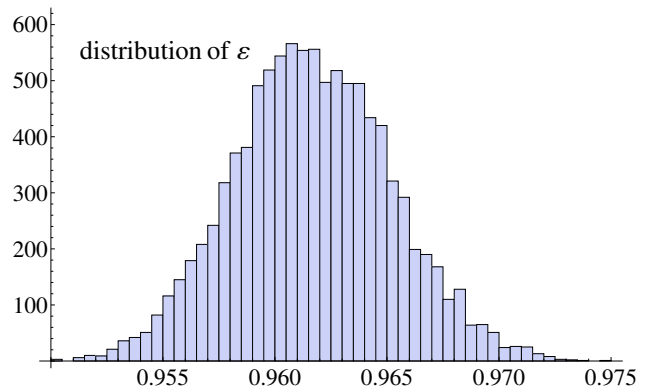


Figure 7: Histogram of 10,000 estimates of ε .

4.2 Clinical Data We test the estimators on representative clinical data. MK-7009 is a potent 3/4A protease inhibitor under development at Merck & Company for the treatment of HCV. MK-7009 is a rapidly reversible non-covalent competitive inhibitor of the non-structural 3/4A protease of the hepatitis C virus. An early phase Ib study with MK-7009 monotherapy administered for 8 days to patients with chronic genotype 1 HCV infection showed potent antiviral activity [12]. Analysis in [13] shows significantly greater viral load declines than from standard of care.

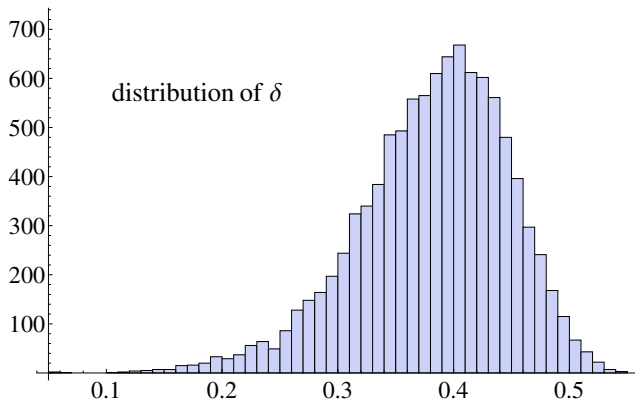


Figure 8: Histogram of 10,000 estimates of δ .

Time series data from 35 patients at doses of 125 mg once-daily (q.d.), 600 mg q.d., 25 mg twice-daily (b.i.d.), 75 mg b.i.d., 250 mg b.i.d., 500 mg b.i.d., or 700 mg b.i.d. have been analyzed. Although few points drop below LOQ in this dataset, full analysis is complicated by the later appearance of mutant viruses with different resistance to the inhibitors [14]. Therefore, another advantage of an early readout of δ is avoidance of effects on viral load by mutant species. We examine a time series from this collection in order to exercise the estimator method for δ using clinical data. We have chosen a single time series from the 500 mg b.i.d. dosing group. The times series for treatment is shown in Figure 9. The series shows a strong biphasic decline that has

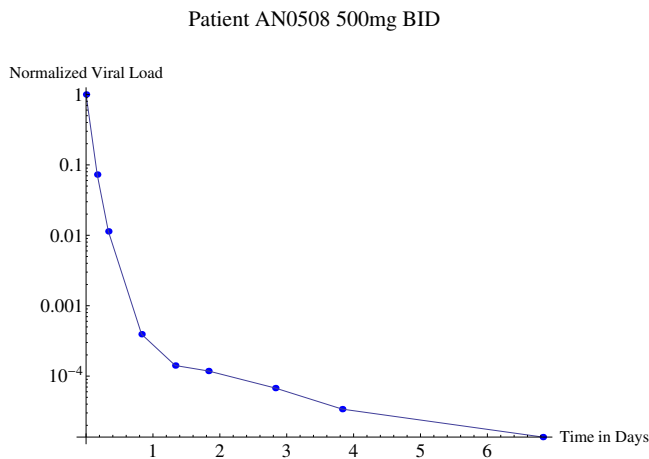


Figure 9: Time series of normalized viral loads during treatment.

no indication of presence of mutant species. In addition, no mutants are detected through a clonal assay.

As before we model the first phase of the decline using the fast solution. The parameters from the first

	Est.	Std. Err.	t Stat.	P-Value
c	13.9500	0.88500	15.77	5.54×10^{-4}
δ	0.4460	0.07600	5.90	9.74×10^{-3}
ε	0.9996	0.00014	7139.90	6.06×10^{-12}

Table 2: Statistics for fit of the regular expansion.

phase are used as an initial guess for the larger models. Figure 10 displays the results of fitting the selected time series data with the regular expansion and the original differential equations. To ensure validity of application of the regular expansion only timepoints less than 2 days are used. There is no such constraint necessary for fitting with the differential equations. However, we observe even using the entire series over 8 days only a very poor fit is attained using all four parameters with the differential equations. As might be expected, the model is insensitive to variation in i_0 . In order to compare fits we arbitrarily set $i_0 = 0.6$. Of note is the overlap of the fits using the differential equations and the regular expansion. Some divergence is seen near the 2 day endpoint. Tables 2 and 3 show statistics for the

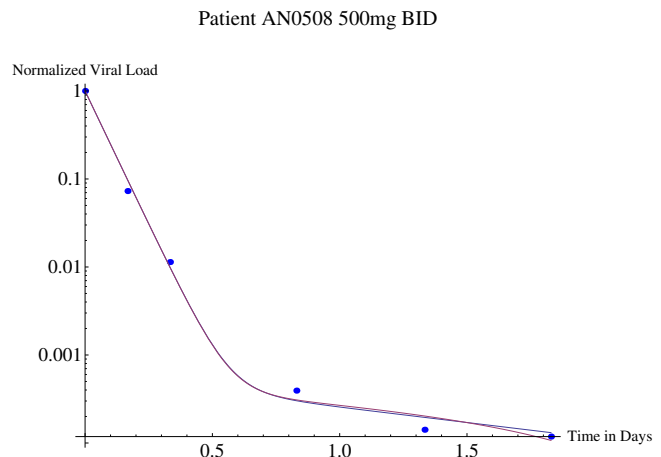


Figure 10: Time series of normalized viral loads during treatment.

model fits shown in figure 10. Much like the synthetic results δ is underestimated by the regular expansion. First phase estimates of ε and c are very similar with good statistics.

Although we show only a single time series, the resulting parameters are representative of the dosing regime. Derived parameters point to a larger viral clearance rate, c , and a greater efficacy, ε , than observed with standard of care. Infected cell clearance rates, δ , are significantly higher than observed with treatment by standard of care. Viral clearance rates and infected

	Est.	Std. Err.	t Stat.	P-Value
c	13.9600	0.7776	117.96	5.65×10^{-5}
δ	0.8000	0.1914	4.20	1.37×10^{-2}
ε	0.9995	0.0002	5972.96	4.71×10^{-15}

Table 3: Statistics for fit of the differential equations with i_0 constrained at 0.6.

cell clearance rates have often previously been assumed to be independent of treatment.

5 Error Estimates

Using monotonicity properties of the solutions to (2.10) and (2.11) we derive estimates for the following error relations when $\varepsilon \geq 0$:

$$(5.50) \quad e_v = v - v^{(0)} - \omega v^{(1)},$$

$$(5.51) \quad e_i = i - i^{(0)} - \omega i^{(1)}.$$

Evolution equations for the errors are

$$(5.52) \quad \frac{de_v}{dt} = -e_v + (1 - \varepsilon)e_i/i_0,$$

$$(5.53) \quad \frac{de_i}{dt} = -\omega e_i + \omega i_0 \left(\frac{v(1-i)}{(1-i_0)} - 1 - \omega v^{(0)} \right),$$

where

$$e_v(0) = e_i(0) = 0.$$

Error bounds derived from (5.52) and (5.53) are

$$(5.54) \quad |e_i| \leq 2i_0(1 - e^{-\omega t}) \sim 2i_0\omega t + O(\omega^2),$$

$$(5.55) \quad |e_v| \leq 2(1 - \varepsilon) \left[1 - e^{-\omega t} - \frac{e^{-\omega t} - e^{-t}}{1 - \omega} \right] \\ \sim 2(1 - \varepsilon)(1 - \omega)t + O(\omega^2).$$

The viral load error grows on the fast time scale while the infected cell fraction error grows on the slower scale. Because of page constraints it will not be possible to give a detailed derivation of these results. Instead, we outline the three major derivation steps in sufficient detail such that the reader may fill in the details. The three steps involved in deriving these estimates are, first, bounding v and i below by 0; second, bounding the derivatives of v and i above by 0; and third, carrying out the estimates.

5.1 Bounds on Functions and Derivatives To bound v below by zero we assume that there is a first time t_1 such that either $v(t_1)$ or $i(t_1)$ or both are 0. Assuming $v(t_1) = 0$ and $i(t_1) > 0$ then at t_1

$$\frac{dv}{dt} = (1 - \varepsilon)i/i_0 > 0.$$

Since $i(t_1) > 0$, by assumption, and $v(t_1)$ is smooth in t there is a time smaller than t_1 , t^* , where $v(t^*) < 0$. Therefore the original assumption leads to a contradiction. A similar argument holds for the case when $i(t_2)$ is zero prior to $v(t_2)$ being 0 for the first time. When both v and i are 0 at the same time, say t_3 for the first time, there is no further change in the solutions from zero since a steady-state has been achieved.

A similar argument by contradiction bounds the derivatives at or below zero. As above there are three cases when one or both of the derivatives first hit zero from below. Assume $i'(t_1) = 0$ and $v'(t_1) < 0$. Using time derivatives of (2.10) and (2.11) we have

$$(5.56) \quad \frac{d^2 i}{dt^2} = \omega i_0 \frac{dv}{dt} \frac{(1-i)}{(1-i_0)} < 0.$$

Again an earlier zero crossing time for $i'(t)$ is indicated, in contradiction to the original assumption. The two other cases follow analogous paths to computations for the functions $v'(t)$ and $i'(t)$.

5.2 Bounds on Errors The solutions to (5.52) and (5.53) may be written implicitly as

$$(5.57) \quad e_i = \omega i_0 e^{-\omega t} \\ \times \int_0^t e^{\omega s} \left(\frac{v(1-i)}{(1-i_0)} - 1 - \omega v^{(0)}(s) \right) ds,$$

$$(5.58) \quad e_v = \frac{(1-\varepsilon)}{i_0} e^{-t} \int_0^t e^s e_i(s) ds.$$

Using bounds computed for v , i and their derivatives, lower and upper bounds are found for $e_i(t)$. The greater of the absolute values of the upper and lower bounds are chosen to determine $|e_i(t)|$. The bound on $|e_i(t)|$ is then used to estimate a bound on $|e_v(t)|$.

We use the bounds on the functions and derivatives in the derivation of bounds on $|e_i(t)|$. The upper and lower bound of $e_i(t)$ are computed and, in this case, a single absolute bound on $|e_i(t)|$ may be found:

$$e_i(t) \leq \omega i_0 e^{-\omega t} \int_0^t e^{\omega s} \left(i/i_0 - 1 - \omega v^{(0)}(s) \right) ds \\ \leq -\omega^2 i_0 e^{-\omega t} \int_0^t e^{\omega s} v^{(0)}(s) ds \\ \leq -\omega^2 i_0 e^{-\omega t} \int_0^t e^{\omega s} ((1-\varepsilon) + \varepsilon e^{-s}) ds \\ = -\omega i_0 (1-\varepsilon)(1 - e^{-\omega t}) + \\ \frac{\omega^2 i_0 \varepsilon}{(1-\omega)} (e^{-t} - e^{-\omega t}).$$

Similarly, a lower bound is estimated as

$$e_i(t) \geq -\omega i_0 e^{-\omega t} \int_0^t e^{\omega s} \left(1 + \omega v^{(0)}(s) \right) ds$$

$$\geq -i_0(1 - e^{-\omega t})(1 + \omega).$$

These results can then be combined, resulting in (5.54). Using (5.54) in (5.58) leads to an estimate for $|e_v(t)|$:

$$\begin{aligned} |e_v(t)| &\leq 2(1 - \varepsilon)e^{-t} \int_0^t (1 - e^{-\omega s})e^s ds \\ &= 2(1 - \varepsilon) \left[(1 - e^{-\omega t}) - \frac{1}{(1 - \omega)} (e^{-\omega t} - e^{-t}) \right]. \end{aligned}$$

Sharper estimates may be found by keeping upper and lower bounds separate. The estimates are sharp enough to represent the asymptotic errors to first order.

6 Conclusions and Acknowledgements

We have outlined the methodology used to derive, analyze and understand approximations to the viral load equations. The resulting hierarchy of approximations and their characterization yields simpler, robust models for appropriate regimes. What has come out of the analysis is nothing less than a series of time intervals where various parameters come into play. Whether the practitioner uses the analytic expansions or numerical methods with appropriate parameters fixed to nominal values, the analysis gives the user confidence they will derive the correct, fitted parameters. We use this hierarchy to find three-parameter fits to data that have few second phase samples before going below LOQ. The techniques described here may be extended to more complicated models that may include multiple viral species or intracellular dynamics.

Overall, the expansions provide insight into how to derive the maximal amount of information from available data within the limits of our current ability to resolve viral loads. Most importantly, we introduce some new analysis methods and machinery for fitting and understanding experimental data enabling accurate decisions about how to treat HCV.

The authors would like to thank the reviewers and editors for their very diligent work. We believe the quality of the paper has been improved in many ways through their efforts.

References

- [1] World Health Organization (WHO). HCV fact sheet. <http://www.who.int/mediacentre/factsheets/fs164/en/>, 2009.
- [2] D. B. Strader, T. Wright, D. L. Thomas, and L. B. Seff. Diagnosis, management, and treatment of hepatitis c. *Hepatology*, 39(4):1147–1171, April 2004.

- [3] B. R. Bacon. Assessing evidence from clinical trials in chronic hepatitis c. *Journal of Viral Hepatitis*, 13(Supplement 1):1–5, 2006.
- [4] K. Gournlain, A. Soulier, B. Pellegrin, M. Bouvier-Alias, C. Hezode, F. Darthuy, J. Remire, and J. M. Pawlotsky. Dynamic range of hepatitis c virus rna quantification with the cobas ampliprep-cobas amplicor hcv monitor v2.0 assay. *J Clin Microbiol.*, 43(4):1669–1673, April 2005.
- [5] A. U. Neumann, N. P. Lam, H. Dahari, D. R. Gretch, T. E. Wiley, T. J. Layden, and A. S. Perelson. Hepatitis c viral dynamics in vivo and the antiviral efficacy of interferon-alpha therapy. *Science.*, 282(5386):103–107, 1998.
- [6] H. Dahari, B. Sainz, A. S. Perelson, and S. L. Uprichard. Modeling subgenomic hepatitis c virus rna kinetics during treatment with alpha interferon. *Journal of Virology*, 83(13):6383–6390, July 2009.
- [7] A. S. Perelson, E. Herrmann, F. Micol, and S. Zeuzem. New kinetic models for the hepatitis c virus. *Hepatology.*, 42(4):749–754, 2005.
- [8] J. Kevorkian and J. Cole. *Multiple Scale and Singular Perturbation Methods*. Springer, New York, 1996.
- [9] J. G. Simmonds and J. E. Mann Jr. *A First Look at Perturbation Theory, 2nd Edition*. Dover, New York, second edition, March 1998.
- [10] G. K. Michalopoulos and M. C. DeFrances. Liver regeneration. *Science.*, 276(5309):60–66, 1997.
- [11] E. A. Coddington and N. Levinson. *A First Look at Perturbation Theory, 2nd Edition*. McGraw-Hill, New York, first edition, 1955.
- [12] E. Lawitz, M. Sulkowski, I. Jacobson, S. Faruqi, W. Kraft, B. Maliakkal, M. Al-Ibrahim, R. Ghalib, S. C. Gordon, P. Kwo, J. Rockstroh, M. Miller, P. Hwang, J. Gress, and E. Quirk. Safety, tolerability and antiviral activity of mk-7009, a novel inhibitor of the hepatitis c virus ns3/4a protease, in patients with chronic hcv genotype 1 infection. In *59th Annual Meeting of the American Association for the Study of Liver Diseases (AASLD)*, November 2008. Abstract 211, Conference Reports for NATAP, <http://www.natap.org/2008/AASLD/AASLD.09.htm>.
- [13] P. Panorchan, R. Nachbar, J. Saltzman, A. K., D. Olsen, E. Quirk, R. Barnard, P. Hwang, H. Wright, and J. A. Stone. Evaluation of the dose-response relationship to short-term monotherapy with the hcv protease inhibitor, mk-7009. In *2nd American Conference on Pharmacometrics (ACoP)*, Mashantucket, Connecticut, October 2009.
- [14] J. A. Stone, P. Panorchan, R. Nachbar, A. Khan, D. Olsen, R. Barnard, P. Hwang, and J. Saltzman. Viral dynamics modeling of viral load and resistance data from short-term monotherapy with the hcv protease inhibitor, mk-7009. In *2nd American Conference on Pharmacometrics (ACoP)*, Mashantucket, Connecticut, October 2009.